IEEE Access
Multidisciplinary | Rapid Review | Open Access Journal

Received June 24, 2020, accepted July 14, 2020, date of publication July 24, 2020, date of current version August 12, 2020.

Digital Object Identifier 10.1109/ACCESS.2020.3011730

Fault Detection Method Using a Convolution Neural Network for Hybrid Active Neutral-Point Clamped Inverters

SANG-HUN KIM, (Graduate Student Member, IEEE), DONG-YEON YOO, (Graduate Student Member, IEEE), SANG-WON AN, (Graduate Student Member, IEEE), YE-SEUL PARK, (Graduate Student Member, IEEE), JUNG-WON LEE, (Member, IEEE), AND KYO-BEUM LEE, (Senior Member, IEEE)

Department of Electrical and Computer Engineering, Ajou University, Suwon 16499, South Korea

Corresponding authors: Kyo-Beum Lee (kyl@ajou.ac.kr) and Jung-Won Lee (jungwony@ajou.ac.kr)

This work was supported by the Ajou University research fund and the National Research Foundation of Korea (NRF) grant funded by the Korea Government (MSIT) (No. 2020R1A2C1007400).

ABSTRACT This article presents an open-switch fault detection method for a hybrid active neutral-point clamped (HANPC) inverter based on deep learning technology. The HANPC inverter generates a three-level output voltage with four silicon switches and two silicon carbide switches per phase. The probability of open fault in switching devices increases because of the large number of switches of the entire power converter. The open-switch fault causes distortion of output currents. A convolution neural network (CNN) comprising several convolution layers and fully connected layers is used to extract features of distorted currents. A CNN network was trained using three-phase current information to determine the location of the open-switch fault. Our proposed CNN model can accurately detect approximately 99.6% of open-switch faults without requiring additional circuitry and regardless of the current level within an average time of 1.027ms. The feasibility and effectiveness of the proposed method are verified by experimental results.

INDEX TERMS Open-switch fault detection, hybrid active neutral-point inverter, silicon carbide, deep learning, convolution neural network.

I. INTRODUCTION

The application of renewable energy-based distributed generation systems for electrical power supply to inhabitants of islands or remote areas has increased in recent years [1]–[2]. Battery energy storage systems (BESSs) are gaining importance because these help to ensure the continuity of energy supply in distributed generation systems. Three-level inverters are generally used in BESSs. These inverters are typical topologies that generate three-level AC output voltage by using high DC voltage sources [3]. Among the many types of three-level inverters, a hybrid active neutral point clamped (HANPC)-type inverter displays high performance during bidirectional operation [4]. The HANPC-type inverter is fabricated with two types of switching devices: Si and SiC power semiconductors [5]. A phase of an HANPC inverter is composed of four Si insulated gate bipolar transistors (IGBTs) and two SiC metal-oxide-semiconductor field-effect transistors (MOSFETs). The HANPC inverter has several advantages including high efficiency, low harmonics, and improved cost-effectiveness.

Notwithstanding these advantages of HANPC inverters, switch failures are likely because of the large number of active switches. The number of active switches in an HANPC inverter is significantly larger than those in other three-level topologies such as neutral-point clamped (NPC)-type, Conergy-NPC-type, or flying capacitor-type inverter [6]–[8]. The use of a larger number of active switches implies a higher probability of switch failure from the perspective of a whole power conditioning system (PCS). The survey on reliability has revealed the percentage distribution of failures in PCSs, and that the probability that all the components of a power device would fail is 31% [9].

The associate editor coordinating the review of this manuscript and approving it for publication was Sze Sing Lee.

Two types of failures are likely in power devices: a short-circuit fault and an open-circuit fault. A short-circuit fault is a state wherein the power transistors maintain the conduction states and are unable to turn off [10]. It causes a rapid increase in the failed phase current and undesirable damage to the other component of the PCS. In contrast, an open-circuit fault implies that the switching device is permanently turned off and the current flow is terminated through a faulty transistor. An open fault results in distortion of the three-phase output currents, i.e., the inverter becomes out of control. This is less dangerous than a short-circuit fault, which needs to be terminated immediately. Thus, it is possible to identify the fault switch in an open-fault scenario and to address the problem by post-fault control. An open switch fault is different from a single current sensor fault. A failure which is occurred in the phase current sensor makes erroneous feedback in an aspect of the entire phase current like a gain drop, miscue in DC offset, or null output. But, an open circuit in single leg leads to a disconnect in switching state level and causes smaller distortion than sensor fault.

Several methods have been proposed to realize open-circuit fault detection in multilevel inverters. In [11], an open-circuit fault detection method for standard NPC inverters was proposed. The pole voltage and duration time can be measured using a comparator circuit to determine the switching state and failure, and failure can be detected within two sampling intervals. Another study proposed a method for fault detection by attaching a current sensor to each ANPC neutral-point branch [12]. A short-circuit or open-circuit fault can be identified by sensing the overcurrent or load current of the circuit using the current sensor. These studies have a problem in that additional sensors or circuits are required for fault detection. To solve this, in a previous study, we proposed a technique to detect open-switch faults in HANPC inverters by observing the distortion of the output current in a stationary reference frame without additional circuitry [13]. To extract the characteristics of the current data, Park's transformation was used to express the three-phase output current as a direct-quadrant (dq) axis current and Park's vector [14] was calculated. The Park's vector rotates about the dq-axis and represents a circular current pattern. The failure of the switch was identified by comparing the radius of the circular pattern drawn by the current and the location of the center point to a specific threshold in the flowchart. However, the failure detection criteria of the flowchart can vary depending on the output current level. Furthermore, an additional switching injection is required to detect the failure of a specific switch, which burdens the circuit.

Several methods for automatically extracting current or voltage characteristics using deep learning have been proposed in recent studies involving open-fault detection. In [15], a method for detecting open-circuit faults using a deep learning approach to the current data output from an AC–DC rectifier has been proposed. First, features of the current data are extracted using a deep belief network (DBN) in which several restricted Boltzmann machines (RBMs) are stacked. The extracted feature finally detects an open-circuit fault through a least-square support vector machine (LSSVM). In [16], the authors studied the detection of open-circuit faults in three-phase full-bridge rectifiers by using sparse autoencoder-based deep neural networks. A failure detection rate of 100% was displayed when the voltage data was learned by constructing a network with two hidden layers.

Convolution neural networks (CNNs), which are among the many learning methods employed for fault detection, extract features of adjacent data using convolution layers. Therefore, learning the three-phase current data together with them is effective for fault detection in HANPC inverters wherein one switch fault affects the current of another circuit. In [17], a deep CNN was trained using the voltage signal as the input data to detect open-circuit faults in the sub-modules of a modular multilevel converter. The average accuracy of the trained model was 98.16%. In addition, the data with white noise were over 20% better than those from previous methods such as support vector machines using a radial basis function (RBF) kernel. In previous studies [13] on fault detection, Park's vector was calculated and the characteristics of the fault signal were extracted through switching injection. However, the neural network assumed that role in [15]–[17]. Furthermore, it could automatically extract features of nonlinear data. However, in [15]–[17], there was a problem in that it does not consider the scenario in which various levels of current are inputted.

In this article, the open-switch fault detection method is proposed. It is based on a CNN algorithm using three-phase current data. The current waveforms are analyzed for each case of open-switch fault in the three-phase HANPC inverter. The current data is acquired in the open-fault scenario of each switching device of the three-phase inverter for various current levels. The learning process primarily involves two steps: 1) pre-processing to determine the normalized patterns of various current levels and 2) training of the fault detection model using CNNs. The trained CNN model can classify the features of each fault case with an accuracy of over 99%. Finally, the validity of the proposed method is demonstrated with the experimental results of a grid-tied HANPC inverter.

II. CIRCUIT CONFIGURATION AND OPERATION OF HANPC INVERTER

A. CIRCUIT CONFIGURATION

Fig. 1 shows representative circuit configurations of the three-level DC–AC inverter. Fig. 1a is a conventional NPC inverter topology with four Si IGBTs and two clamping diodes. The conventional NPC inverter was proposed in the 1980s to reduce the harmonics of motor drive systems. Extensive research has yielded NPC inverters displaying improved DC-link voltage balance and operation in the overmodulation region [18]–[21]. NPC inverters exhibit the disadvantage of unequal power loss during bidirectional operation [22]. When the energy is transformed from DC to AC, the switching losses of the four Si IGBTs are significantly higher in the

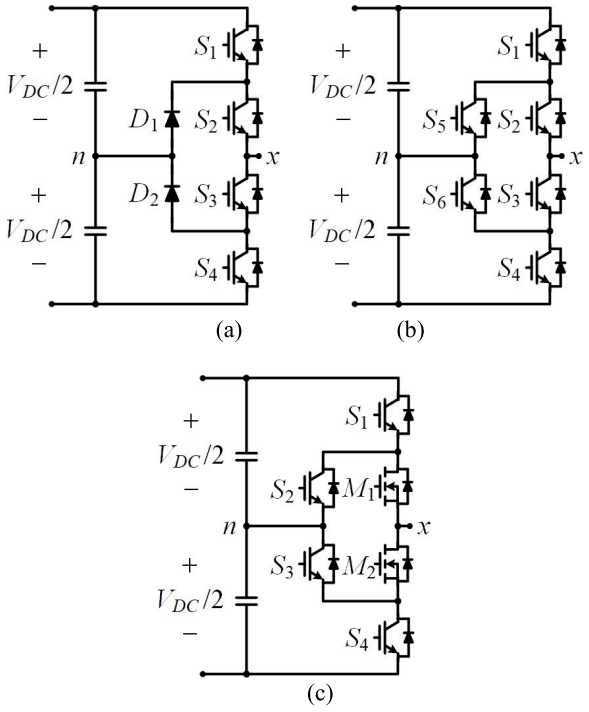

FIGURE 1. Typical circuit types of three-level inverters, (a) NPC-type, (b) ANPC-type, (c) HANPC-type.

outer switching devices (S_1 and S_4) than in the inner switching devices (S_2 and S_3) [23]. In contrast, when the energy is transformed from AC to DC, the inner switching devices display high switching losses. The unbalanced power loss causes unequal heat dissipation from the individual power device of a PCS and degrades the device's characteristics. Thereby, the maximum permissible temperature limits the switching frequency and the entire output power of the PCS [24].

Fig. 1b shows the active NPC (ANPC) inverter topology with six Si IGBTs. The ANPC inverter was proposed in [23] by replacing two diodes with active switches (IGBTs) to overcome the non-uniform loss distribution of each switch. The ANPC inverter can combine current commutations with various switching states. However, it is controlled using an intricate modulation strategy [23]–[25].

Fig. 1c shows a single-phase circuit configuration of HANPC inverters. As shown in Fig. 2, the grid-tied HANPC inverter can transfer electrical energy from a DC battery to a three-phase grid and vice versa. The HANPC inverter is a good solution for achieving low power loss and uniform loss distribution during bidirectional operation. This result is attained by incorporating a SiC transistor in the HANPC inverter. SiC is one of the prominent wide bandgap (WBG) materials that enable operation at a higher voltage and temperature with increased efficiency [26]–[27]. However, the application of SiC devices to each switch is uneconomical because of the high price of WBG devices [5]. A leg of the HANPC inverter consists of two SiC MOSFETs and four Si IGBTs. The switching loss can be limited to two SiC MOSFETs of the HANPC inverter by using an appropriate

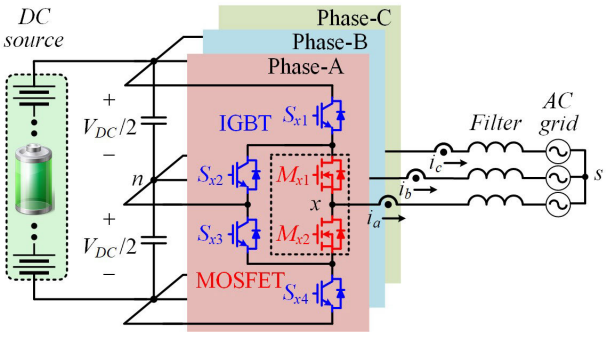

FIGURE 2. Circuit configuration of grid-tied HANPC inverter.

modulation method. The fundamental modulation method of the HANPC inverter is introduced in the following section.

B. MODULATION METHOD

Fig. 3 presents two switching frequency waveforms that are utilized in HANPC inverters: low frequency (LF) and high frequency (HF). LF/HF pulse width modulation (PWM) is implemented for an HANPC inverter in a few steps. As shown in Fig. 3a, a reference voltage (V^*_{xs}) is set for each phase of an HANPC inverter, and an offset voltage (V_{offset}) is injected to realize space vector PWM. After generating the reference pole voltage (V^*_{xn}), the reference signal is normalized ($V^*_{xn(norm)}$) to be compared with a triangular carrier signal (V_{tri}), as shown in Fig. 3b. Fig. 3c and Fig. 3d show the LF/HF PWM signals (V_{GE}, V_{GS}) that are produced by comparing the reference and carrier signals in the previous step. The LF and HF PWM signals are used to turn on and off the Si IGBTs and SiC MOSFETs, respectively. Finally, as shown in Fig. 3e, the output pole voltage (V_{xn}) is generated as a three-level waveform ($+V_{DC}/2$, 0, and $-V_{DC}/2$).

TABLE 1. Switching states and output pole voltage (1: turn on, 0: turn off).

Switching States	S_1	S_2	S_3	S_4	M_1	M_2	Output Voltage
Positive (P)	1	1	0	0	1	0	$+V_{DC}/2$
Zero (O+)	1	1	0	0	0	1	0
Zero (O–)	0	0	1	1	1	0	0
Negative (N)	0	0	1	1	0	1	$-V_{DC}/2$

Fig. 4 and TABLE 1 present the output pole voltages and current flows for each switching state of an HANPC inverter. In Fig. 4, the red highlighted switch refers to the turned-on states whereas the black ones refer to the turned off states. Meanwhile, the blue dotted line illustrates the current flow for each switching state. The HANPC inverter is presented as four switching states depending on the turned on and off states of each switch. As illustrated in Fig. 4a and TABLE 1, the output voltage is $+V_{DC}/2$ when the switching state is positive (P). The phase current is conducted through the two upper switches in the P switching state. Fig. 4b and Fig. 4c

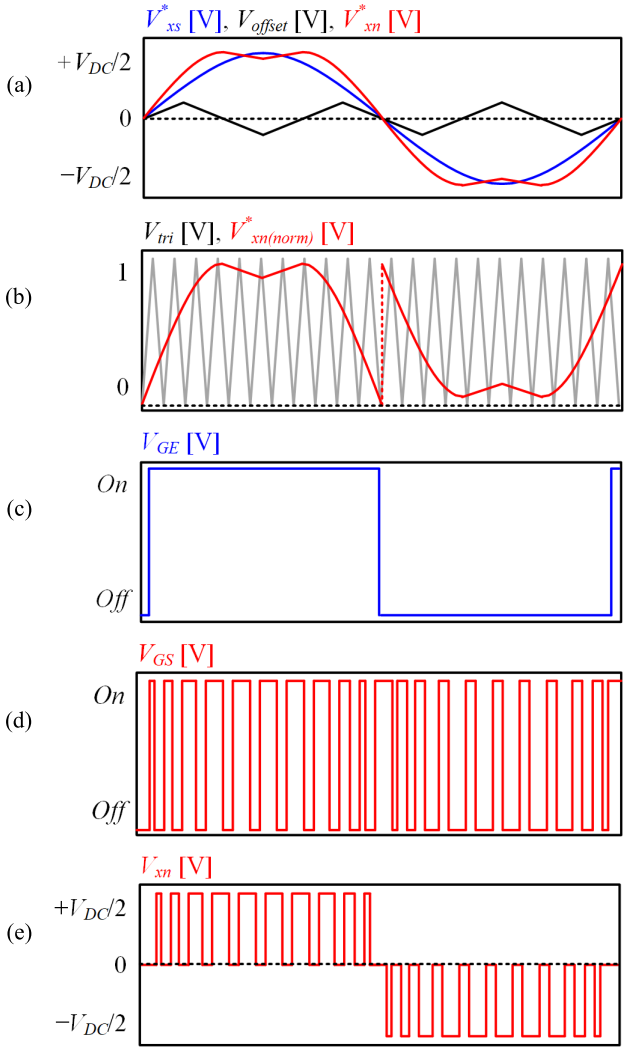

FIGURE 3. Modulation method of HANPC inverters, (a) Reference voltage and offset voltage for SVPWM, (b) Triangular carrier waveform and normalized reference voltage, (c) LH PWM signal for Si IGBTs, (d) HF PWM signal for SiC MOSFETs, (e) Output pole voltage.

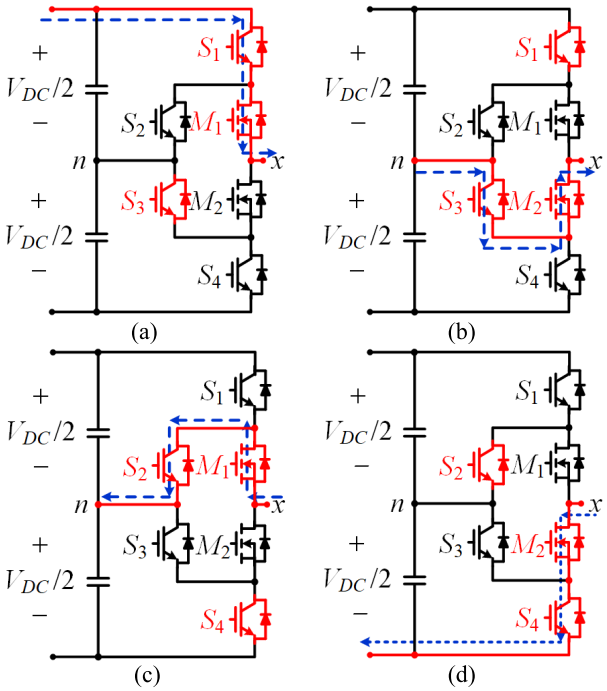

FIGURE 4. Switching states and current path of HANPC inverter, (a) P state, (b) O+ state, (c) O– state, (d) N state.

show that there are two zero switching states (O+, O–) for zero output voltage. In the O+ state, the output current flows from the DC neutral point to the AC side via the neutral point IGBT (S_3) and downside MOSFET (M_2). In the other zero state (O–), the conduction direction is opposite, and the neutral point IGBT (S_2) and upside MOSFET (M_1) are turned on. Finally, Fig. 4d represents a negative (N) switching state for a negative output voltage. In the N switching state, the two lower switches and neutral point switch turn on, and a negative current flows down from the AC side to the DC side.

The four switching states are separated by a reference voltage value. The switching states of the HANPC inverter when the reference voltage is positive are P or O+. This implies that the output pole voltage is $+V_{DC}/2$ or 0. Meanwhile, when the reference voltage is negative, the switching state of an HANPC inverter is N or O–, and the output pole voltage is $-V_{DC}/2$ or 0. The changeover from the P state to the O+ states occurs when the two MOSFETs are turned on and off complementarily while the other switches (IGBTs, S_1 and S_3) maintain their states. The relationship between the N states and O– states also involves similar complementary operations of MOSFETs. In the HANPC inverter, the neutral clamped switches (S_2 and S_3) are turned on even P or N state. These IGBT switches are used in two zero (O+ and O–) states according to turning on and off by the MOSFET switches. In this way, the HANPC inverter operates in reduced switching loss in IGBT switches.

III. OPEN FAULT DETECTION BY CONVOLUTION NEURAL NETWORK

A. ANALYSIS OF OPEN FAULT HANPC INVERTER

Fig. 5 shows the open-switch fault in an HANPC inverter for each single switching device. If the open fault occurs in the upper switches (IGBT S_1 or MOSFET M_1) as shown in Fig. 5a, the P state is not viable, and the positive current is not generated completely as an A-phase current. Fig. 5b and Fig. 5c show the failure of neutral point switches. In this case, it is incapable of creating O switching states. The current path is disconnected because of the open fault of the inner-side IGBTs, as shown in Fig. 5b and Fig. 5c. The absence of an O+ or O– state distorts the positive or negative side current flow, respectively. As shown in Fig. 5d, the open failure of the lower switches (IGBT S_4 or MOSFET M_2) results in the incapability of creating an N switching state, which, in turn, results in the aspect opposite to that of the upper switch fault. The negative current cannot be generated entirely by the open circuit of the faulty leg of the HANPC inverter without

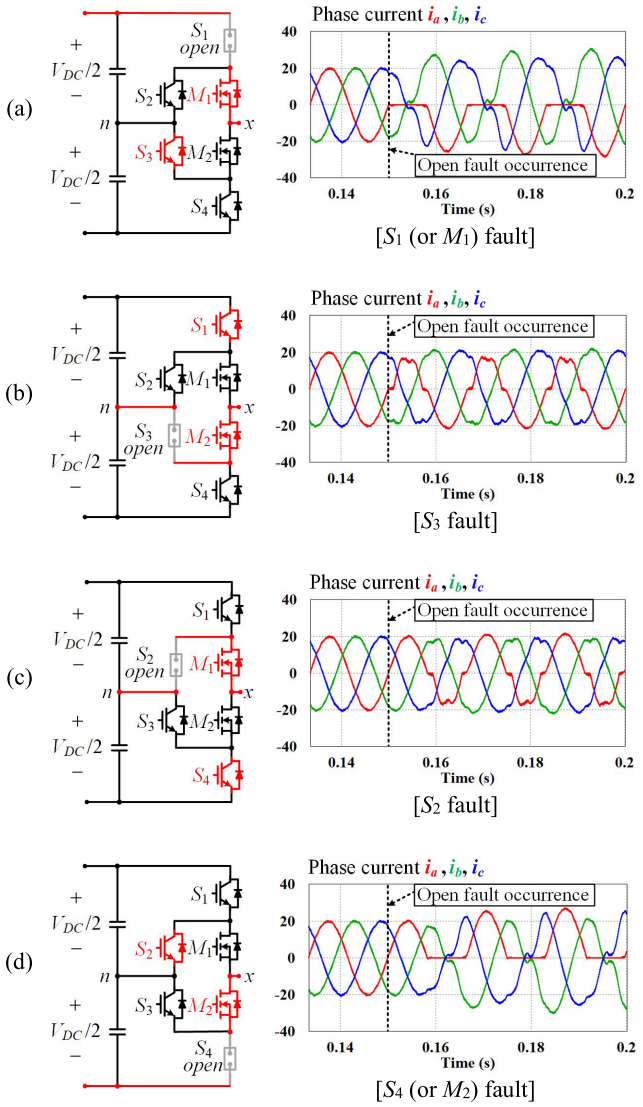

FIGURE 5. Open fault states in A-phase and three-phase current waveforms of HANPC inverter, (a) when the fault occurred in IGBT S_1 or MOSFET M_1, (b) when the fault occurred in IGBT S_3, (c) when the fault occurred in IGBT S_2, (d) when the fault occurred in IGBT S_4 or MOSFET M_2.

affecting the positive current of the A-phase. Thus, six open fault cases are considered for single switches, and eighteen cases are feasible for a three-phase HANPC inverter.

As listed in Fig. 5, the output phase current waveforms are classified into four cases for a single open fault in each phase of an HANPC inverter. A single open fault that occurs in the IGBT S_1 or MOSFET M_1 causes a similar current distortion as shown in Fig, 5a. Meanwhile, a single fault in the IGBT S_4 or MOSFET M_2 generates similar features of output current. A special switching scheme for identifying faults in S_1 and M_1 (or S_4 and M_2) was proposed in [13] and [28]. Previous works used delicate detection methods because of the uncertainty of open-switch faults. As mentioned in [28], the forced switching state is necessary for identifying faulty switches. However, the forced switching state causes the generation of the peak current, which can impair the switching devices. Thus, the proposed open fault detection is accomplished for each switches' fault by a deep learning approach and without other switching skills.

B. FAULT DETECTION MODEL CONSTRUCTION

1) PRE-PROCESSING TO DETERMINE THE NORMALIZED PATTERNS FROM VARIABLE CURRENT LEVELS

The three-phase current data are shown in a repetitive pattern in Fig. 5, and this pattern can appear at various current levels. Even when a failure occurs in a switch in the same position, the current data may display different patterns owing to the current level. This can adversely affect learning. In addition, it is necessary to transform the raw current data measured in the inverter into a form that can be input to the learning network. In this study, the raw current data are transformed into a form that can be used for learning through two pre-processing steps. The raw data in Fig. 6 are of the three-phase current and the phase angles of the A-phase current. These undergo a conversion process that identifies a normalized current pattern such that it is unaffected by the current level and divides the data according to the period.

a: DATA NORMALIZATION

The first pre-processing step is the normalization of current data obtained from experiments with different current levels. The three-phase current data are normalized through division by the current level in each experiment. Two examples of the current levels (5 A, 9 A) are shown in Fig. 6, and the current data are divided according to the respective current levels.

b: DATA GENERATION FOR LEARNING

The second pre-processing step divides the current data showing repetitive patterns into one cycle unit. The phase angle of the A-phase current increases from –Pi to +Pi for one period. Therefore, the three-phase current data can be divided into units of one cycle each if the division is based on the point where the phase angle of the A-phase becomes –Pi. The divided current data is in the form of a 3 × N matrix, and are used as input data for an open-switch fault detection network. Here, N represents the number of current data measured during one cycle.

2) CNN-BASED FAULT DETECTION MODEL

There are 18 open-switch fault cases to be detected in this study. The proposed method detects whether the three-phase circuits composed of six switches (S_{1-4}, M_{1-2}) have failed. Nineteen cases (the 18 switch failure cases and the case of normal operation) were set as the classification result of the learning model, i.e., the class labels. The proposed CNN automatically extracts the characteristics of the three-phase current from the input data and classifies it as one of the 19 labels. The CNN consists of two convolution layers and two fully connected layers, as shown in Fig. 7. The three-phase current data are input in the form of a 3 × 100 matrix when the current data are measured 100 times in one cycle. The input matrix

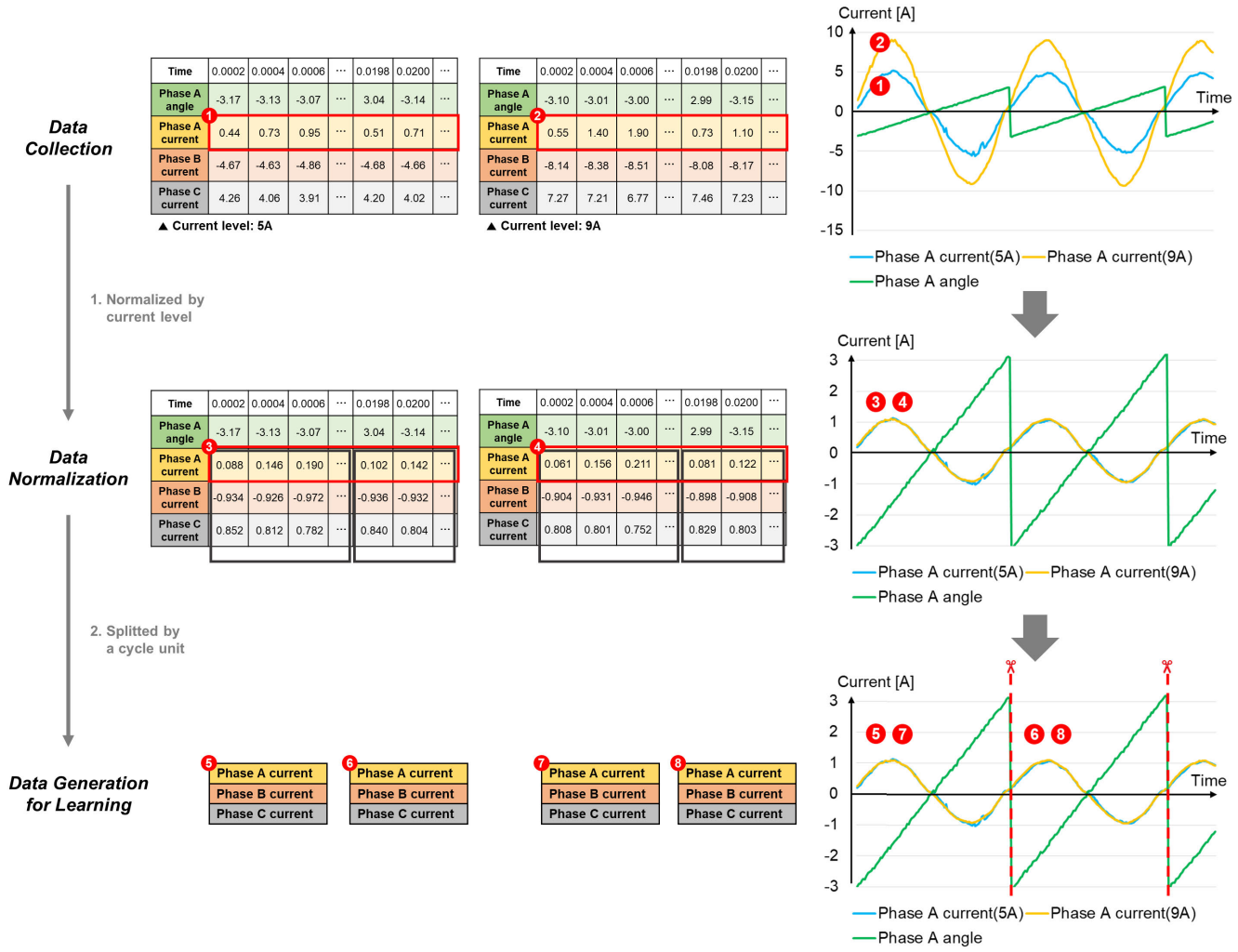

FIGURE 6. Determination of the normalized patterns from three-phase current waves (time unit: s, angle unit: rad, current unit: A).

passes through two convolution layers using a 3 × 3 kernel. The numbers of channels in the convolution layers are 32 and 64. Furthermore, these are set to identical stride (1, 1) and padding. It passes through a max pooling layer with a kernel size of 1 × 2, after each convolution layer.

Next, it passes through two fully connected layers to determine the location of the faulty switch. After it passes through the first fully connected layer, 1,024 hidden units are created from the feature map. Nineteen values are generated as outputs while it passes through the second fully connected layer. These outputs indicate the probability of normal operation and the 18 switch failure labels. The label with the highest probability among the outputs is the classification result of the input data. The dropout was set to 0.5 to prevent overfitting of the learning model, and a rectified linear unit was used as an activation function. Learning was performed using a backpropagation method that calculates the error of the actual correct answer and inference and feeds the weight of the network in the direction in which the error decreases. The cross entropy is used as the loss function.

TABLE 2. Experimental parameters.

Parameters	Value	Unit
Voltage of DC-link (V_{DC})	600	V
Line-to-line grid voltage	380	V_{rms}
Capacitance of DC-link	4,700	μF
Filter inductance	1	mH
Switching frequency of SiC-MOSFETs (HF)	20,000	Hz
Switching frequency of Si-IGBTs (LF)	50	Hz

IV. EXPERIMENTAL RESULTS

A. EXPERIMENTAL SETUP

Fig. 8 and TABLE 2 present an experimental set-up and parameters, respectively, of the grid-tied three-phase HANPC inverter. Several experiments were performed to demonstrate the effectiveness of the proposed method for identifying open

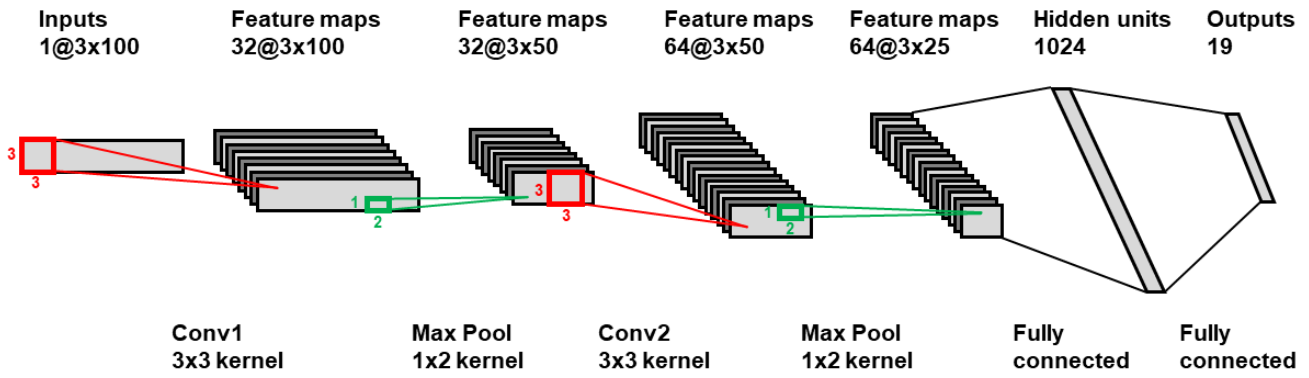

FIGURE 7. Convolution neural network structure for three-phase current data learning.

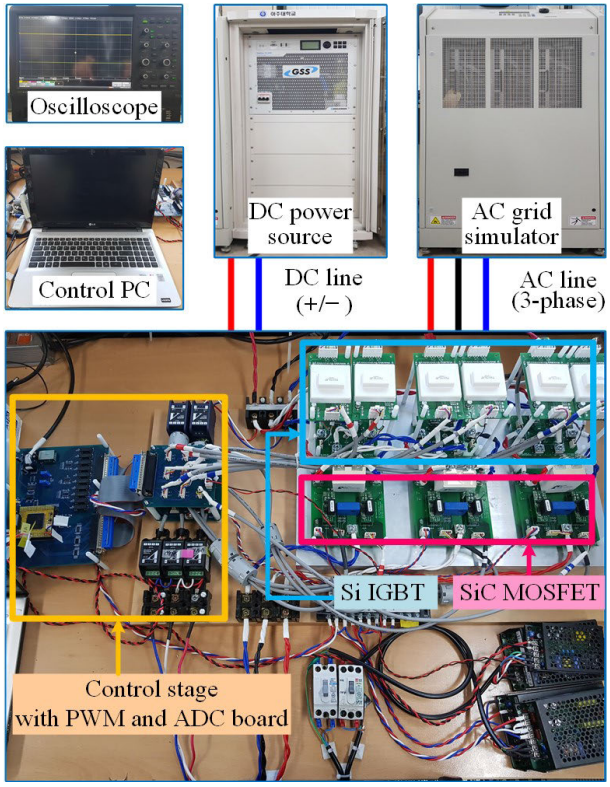

FIGURE 8. Experimental setup of HANPC inverter.

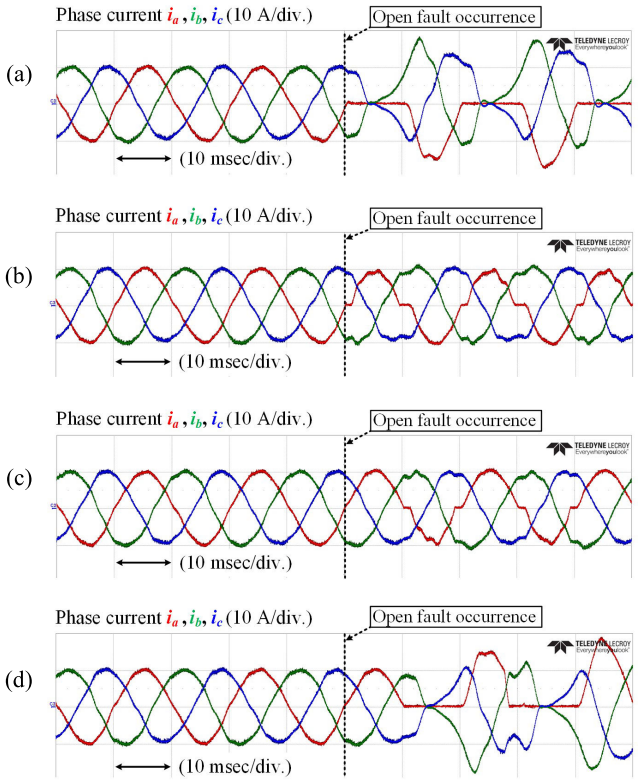

FIGURE 9. Three-phase current waveforms of HANPC inverter for the open fault in A-phase, (a) Fault occurred at switch S_1 (or M_1), (b) Fault occurred at switch S_3, (c) Fault occurred at switch S_2, (d) Fault occurred at switch S_4 (or M_2).

fault switches in the HANPC inverter. The experimental set-up comprises the following parts: the three-phase HANPC inverter, a control board DC power source (TC.P.20.600.400 of REGATRON), and AC grid simulator (MX30 of California Instruments). The HANPC inverter is composed of three Si IGBT modules (SK75GBB066T of Semikron) and six discrete-type SiC MOSFET switches (C2M0040120D of CREE) with appropriate gate driver units. The control board is based on a digital signal processor (TMS320F28377S of Texas Instruments), which has the functionalities of PWM and analog-to-digital conversion (ADC). An oscilloscope (HDO6104 of Teledyne LeCroy) was used to capture and save the instantaneous current values of the three-phase HANPC inverter.

Fig. 9 shows the three-phase current waveforms of the HANPC inverter after the open fault had occurred in the A-phase. The output current of the A-phase started to distort after the occurrence of the open fault. As presented in Fig. 9a, when the open fault occurred in S_1 or M_1, the positive range of the A-phase current disappeared, whereas the other phase currents fluctuated. In contrast, the lower switch fault (S_4 or M_2) worsened the negative currents, as shown in Fig. 9d. In the other cases, the neutral point switches (S_2 or S_3) causes a marginal distortion in the A-phase current as shown in Fig. 9c and Fig. 9d, respectively.

B. FAULT DETECTION OF SINGLE-LEVEL CURRENT

First, the trained model was evaluated using the failure detection result of a single-level current wherein the current is not normalized. It was trained with an output current level of 5 A. The current was measured for 100 cycles with either normal operation or a specific switch failure from among the 18 switches. A hundred three-phase current data matrices were obtained in each experiment, and a total of 1,900 ($1 \times 19 \times 100$) matrices were generated. The dimensions of each current data matrix were 3×100. The ratio of the train and test data was set to 9:1 with reference to the general 10-fold cross validation method, and 1,710 and 190 matrices were used as the training and test data, respectively, for learning. The batch size was set to 500, and the model was trained for 10,000 iterations.

TABLE 3. Accuracy of three-phase current data (multi-level) using CNN.

Number of iterations	Train accuracy	Test accuracy
1,000	1.000	1.000
2,000	1.000	1.000
3,000	1.000	1.000
4,000	1.000	1.000
5,000	1.000	1.000
6,000	1.000	1.000
7,000	1.000	1.000
8,000	0.056	0.053
9,000	0.052	0.053
10,000	0.048	0.053

TABLE 3 presents the training and test accuracy for the detection of open-switch faults from single-level current data according to the number of iterations. The training accuracy represents the fault detection performance of the model that was evaluated with the training dataset used for the model training. The test accuracy represents the fault detection accuracy evaluated using a test dataset that was not used for learning. The model takes 1.027ms on average time for open-switch fault detection of pre-processed test data and has training and test accuracy of 1.000 even with 1,000 iterations, i.e., it accurately detects all three-phase switch failures. However, underfitting (where the training and test accuracies are lowered) was observed for 8,000 or more iterations (in TABLE 3). The model validation related to this problem is discussed toward the end of this section.

C. FAULT DETECTION OF MULTI-LEVEL CURRENT

The learning data were generated by experimenting with 11 current levels from 5 A to 15 A. The current was measured for 100 cycles with normal operation or a specific switch failure from among the 18 switches, as described in the previous section. This was repeated for each current level. A hundred three-phase current data matrices were obtained in an experiment, and a total of 20,900 ($11 \times 19 \times 100$) matrices were generated. The ratio of the training and test data was set to 9:1, and 18,810 and 2,090 matrices were used as training and test data, respectively, for learning. The batch size was set to 500, and the model was trained for up to 10,000 iterations.

TABLE 4. Performance of open-switch fault detection using CNN (Iteration 5,000).

Number of iterations	Train accuracy	Test accuracy
1,000	0.972	0.971
2,000	0.986	0.984
3,000	0.996	0.988
4,000	0.990	0.991
5,000	0.998	0.994
6,000	0.046	0.053
7,000	0.054	0.053
8,000	0.054	0.053
9,000	0.040	0.053
10,000	0.070	0.053

TABLE 4 presents the open-switch fault detection accuracy of the multi-level current data according to the number of iterations. The model displays a high training accuracy of 0.972 even with 1,000 iterations, and the highest training accuracy of 0.998 at 5,000 iterations. The highest test accuracy was 0.994 at 5,000 iterations, and this corresponded to the highest training accuracy. TABLE 5 presents the performance of the trained model with 5,000 iterations. Precision, recall, and F1-score, which were used as the performance verification indicators, are illustrated in Fig. 10.

		True condition	
		Positive	**Negative**
Predicted condition	**Positive**	True positive (TP)	False positive (FP)
	Negative	False negative (FN)	True negative (TN)

$$Accuracy = \frac{TP + TN}{TP + FP + FN + TN}$$

$$Precision = \frac{TP}{TP + FP}, \quad Recall = \frac{TP}{TP + FN}$$

$$F1\text{-}score = \frac{2}{Precision^{-1} + Recall^{-1}}$$

FIGURE 10. Indicators used to evaluate learning performance- precision, recall, F1-score.

Precision refers to the ratio of data that are actual failures from among those that were predicted to be failures by the

TABLE 5. Performance of open-switch fault detection using CNN (Iteration 5,000).

Fault type	Precision	Recall	F1-score
Normal	0.991	1.000	0.991
A-phase S_1	0.991	0.991	0.991
A-phase S_2	0.991	0.991	0.991
A-phase S_3	0.917	1.000	0.957
A-phase S_4	1.000	0.909	0.952
A-phase M_1	1.000	1.000	1.000
A-phase M_2	1.000	0.991	0.995
B-phase S_1	1.000	1.000	1.000
B-phase S_2	1.000	1.000	1.000
B-phase S_3	1.000	1.000	1.000
B-phase S_4	1.000	1.000	1.000
B-phase M_1	1.000	1.000	1.000
B-phase M_2	1.000	1.000	1.000
C-phase S_1	1.000	1.000	1.000
C-phase S_2	1.000	1.000	1.000
C-phase S_3	1.000	1.000	1.000
C-phase S_4	1.000	1.000	1.000
C-phase M_1	1.000	1.000	1.000
C-phase M_2	1.000	1.000	1.000

algorithm. Recall refers to the ratio of data that were predicted to be failures from among the actual failure data. In general, the precision and recall are inversely proportional, and the F1-score is calculated as the harmonic mean of the two indicators. Of the 2,090 sets of test data, 13 faults were incorrectly detected, i.e., the test accuracy was 0.994. From among the switches of the A-phase circuit that failed detection, the lowest recall was that of S_4 (0.909). However, the precision, recall, and F1-score of the A-phase circuit were 0.9 or higher. All the failures were successfully detected in the case of the B·C-phase circuit. Furthermore, the performance was 1.000 for all the indicators. Similarly, to single-level current, underfitting was observed for 6,000 or more iterations (in TABLE 4). The model validation pertaining to this problem is discussed in the following section.

D. MODEL VALIDATION

Underfitting can be observed in the case of 8,000 iterations in TABLE 3 or 6,000 iterations in TABLE 4. To examine the effect of the ratio of training and test data on the learning performance, a stability validation experiment was also performed by setting the ratio of the two datasets differently. In the validation experiment, the ratio of test data was varied from 10% (training data 90%, test data 10%) to 50% (training data 50%, test data 50%). Learning was performed 20 times independently, and the instances at which underfitting occurred were recorded.

TABLE 6. Number of first occurrences of underfitting in a specific iteration according to the test ratio (experiment repeated 20 times).

Number of iterations	Test ratio				
	10%	20%	30%	40%	50%
1,000	0	0	0	0	0
2,000	0	0	0	0	0
3,000	0	0	0	0	0
4,000	0	0	1	0	0
5,000	2	3	5	4	3
6,000	11	15	3	11	5
7,000	6	1	10	4	8
8,000	1	1	0	1	4
9,000	0	0	1	0	0
10,000	0	0	0	0	0
Average test accuracy	0.996	0.998	0.998	0.997	0.998

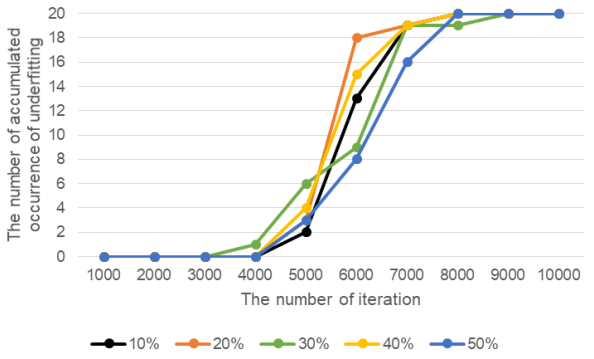

FIGURE 11. Accumulated number of underfitting occurrences according to the test ratio and iteration.

Fig. 11 shows the cumulative value of the experiment (from among the 20 experiments) in which underfitting appeared in each iteration, for the different test ratios. Underfitting occurred from 4,000 iterations for a test ratio of 30%. Furthermore, underfitting always occurred when the number of iterations was over 5,000 in the experiments for all the test ratios. In particular, the occurrence of underfitting rapidly increased from 5,000 to 7,000 iterations. TABLE 6 presents the sum of the iterations at the first occurrence of underfitting, when the accuracy is measured for every 1,000 iterations. The number of iterations at which underfitting occurred for the first time in each experiment varied from 4,000 iterations to 9,000 iterations. It appears that underfitting is not caused by an imbalance of data because iterations that correspond to underfitting are not skewed even when the ratio of test data

is varied. In addition, 3,000 iterations without underfitting displayed a test accuracy of at least 0.979 (average precision = 0.986, average recall = 0.986, and average F1-score = 0.986) and a high performance with fewer iterations.

The average test accuracy was higher than 0.996 for all the ratios when the highest accuracy was calculated before underfitting occurred. Therefore, when learning for fault detection, the performance of the network is not significantly affected by the test ratio. In addition, a suitable performance is guaranteed even with a stable 3,000 iteration model displaying underfitting problems.

V. CONCLUSION

This article proposes a neural network approach about open-switch failure of grid-tied HANPC inverters. The HANPC inverter generates high-quality sinusoidal output currents with remarkable efficiency during bidirectional operation. The open-switch fault of the HANPC inverter resulted in the distortion of the three-phase output current. There are six types of single fault for each phase of an HANPC inverter and eighteen cases for the three-phase system. In each case, a CNN was applied to train the feature of the current waveform. The trained neural network displayed a high average detection accuracy of 99.6% for multi-level current open-switch faults within an average time of 1.027ms. The experiments were conducted to verify the performance of the proposed fault detection method.

ACKNOWLEDGMENT

(Sang-Hun Kim and Dong-Yeon Yoo are co-first authors.)

REFERENCES

[1] K.-B. Lee and J.-S. Lee, *Reliability Improvement Technology for Power Converters*. Singapore: Springer, 2017.

[2] M. Liserre, T. Sauter, and J. Hung, "Future energy systems: Integrating renewable energy sources into the smart power grid through industrial electronics," *IEEE Ind. Electron. Mag.*, vol. 4, no. 1, pp. 18–37, Mar. 2010.

[3] M. Bragard, N. Soltau, S. Thomas, and R. W. De Doncker, "The balance of renewable sources and user demands in grids: Power electronics for modular battery energy storage systems," *IEEE Trans. Power Electron.*, vol. 25, no. 12, pp. 3049–3056, Dec. 2010.

[4] B. H. Kwon, S.-H. Kim, K.-C. Bae, and K.-B. Lee, "Performance analysis on a bidirectional operation of a three-level hybrid ANPC inverter," *Trans. Korean Inst. Electr. Engineers*, vol. 68, no. 10, pp. 1204–1213, Oct. 2019.

[5] Q.-X. Guan, C. Li, Y. Zhang, S. Wang, D. D. Xu, W. Li, and H. Ma, "An extremely high efficient three-level active neutral-point-clamped converter comprising SiC and Si hybrid power stages," *IEEE Trans. Power Electron.*, vol. 33, no. 10, pp. 8341–8352, Oct. 2018.

[6] A. Nabae, I. Takahashi, and H. Akagi, "A new neutral-point-clamped PWM inverter," *IEEE Trans. Ind. Appl.*, vol. IA-17, no. 5, pp. 518–523, Sep. 1981.

[7] J. Rodriguez, J.-S. Lai, and F. Zheng Peng, "Multilevel inverters: A survey of topologies, controls, and applications," *IEEE Trans. Ind. Electron.*, vol. 49, no. 4, pp. 724–738, Aug. 2002.

[8] P. Knaup, "Inverter," International Patent Application WO 200 704 420 A1, May 3, 2007.

[9] S. Yang, A. Bryant, P. Mawby, D. Xiang, L. Ran, and P. Tavner, "An industry-based survey of reliability in power electronic converters," *IEEE Trans. Ind. Appl.*, vol. 47, no. 3, pp. 1441–1451, May 2011.

[10] U.-M. Choi, F. Blaabjerg, and K.-B. Lee, "Study and handling methods of power IGBT module failures in power electronic converter systems," *IEEE Trans. Power Electron.*, vol. 30, no. 5, pp. 2517–2533, May 2015.

[11] T.-J. Kim, W.-C. Lee, and D.-S. Hyun, "Detection method for open-circuit fault in Neutral-Point-Clamped inverter systems," *IEEE Trans. Ind. Electron.*, vol. 56, no. 7, pp. 2754–2763, Jul. 2009.

[12] P. Fazio, M. Marchesoni, and G. Parodi, "Fault detection and reconfiguration strategy for ANPC converters," in *Proc. 15th Int. Power Electron. Motion Control Conf. (EPE/PEMC)*, Sep. 2012, Art. no. DS1b.17-1-DS1b.17-5

[13] B. H. Kwon, S.-H. Kim, S.-M. Kim, and K.-B. Lee, "Fault diagnosis of open-switch failure in a grid-connected three-level Si/SiC hybrid ANPC inverter," *Electron.*, vol. 9, no. 399, pp. 1–18, Feb. 2020.

[14] A. J. M. Cardoso and E. S. Saraiva, "Computer-aided detection of air-gap eccentricity in operating three-phase induction motors by Park's vector approach," *IEEE Trans. Ind. Appl.*, vol. 29, no. 5, pp. 897–901, Sep./Oct. 1993.

[15] T. Shi, Y. He, T. Wang, and B. Li, "Open switch fault diagnosis method for PWM voltage source rectifier based on deep learning approach," *IEEE Access*, vol. 7, pp. 66595–66608, 2019.

[16] L. Xu, M. Cao, B. Song, J. Zhang, Y. Liu, and F. E. Alsaadi, "Open-circuit fault diagnosis of power rectifier using sparse autoencoder based deep neural network," *Neurocomputing*, vol. 311, pp. 1–10, Oct. 2018.

[17] X. Qu, B. Duan, Q. Yin, M. Shen, and Y. Yan, "Deep convolution neural network based fault detection and identification for modular multilevel converters," in *Proc. IEEE PESGM Conf.*, Aug. 2018, pp. 1–5.

[18] S.-W. Hyun, S.-J. Hong, J.-H. Lee, C.-B. Lee, and C.-Y. Won, "A method to compensate the distorted space vectors in the unbalanced neutral point voltage of 3-level NPC PWM inverters," *J. Power Electron.*, vol. 16, no. 2, pp. 455–463, Mar. 2016.

[19] J.-H. Jung, J.-H. Park, J.-M. Kim, and Y.-D. Son, "DC-link voltage balance control using fourth-phase for 3-phase 3-level NPC PWM converters with common-mode voltage reduction technique," *J. Power Electron.*, vol. 19, no. 1, pp. 108–118, Jan. 2019.

[20] D.-M. Lee, J.-W. Jung, and S.-S. Kwa, "Simple space vector PWM scheme for 3-level NPC inverters including the overmodulation region," *J. Power Electron.*, vol. 11, no. 5, pp. 688–696, Sep. 2011.

[21] J.-S. Lee and K.-B. Lee, "Open-circuit fault-tolerant control for outer switches of three-level rectifiers in wind turbine systems," *IEEE Trans. Power Electron.*, vol. 31, no. 5, pp. 3806–3815, May 2016.

[22] J. Rodriguez, S. Bernet, P. K. Steimer, and I. E. Lizama, "A survey on neutral-point-clamped inverters," *IEEE Trans. Ind. Electron.*, vol. 57, no. 7, pp. 2219–2230, Jul. 2010.

[23] T. Bruckner, S. Bernet, and H. Guldner, "The active NPC converter and its loss-balancing control," *IEEE Trans. Ind. Electron.*, vol. 52, no. 3, pp. 855–868, Jun. 2005.

[24] T. Bruckner, S. Bernet, and P. K. Steimer, "Feedforward loss control of three-level active NPC converters," *IEEE Trans. Ind. Appl.*, vol. 43, no. 6, pp. 1588–1596, 2007.

[25] D. Floricau, E. Floricau, and G. Gateau, "Three-level active NPC converter: PWM strategies and loss distribution," in *Proc. 34th Annu. Conf. IEEE Ind. Electron.*, Nov. 2008, pp. 3333–3338.

[26] J. Millán, P. Godignon, X. Perpiñà, A. Pérez-Tomás, and J. Rebollo, "A survey of wide bandgap power semiconductor devices," *IEEE Trans. Power Electron.*, vol. 29, no. 5, pp. 2155–2163, May 2014.

[27] G. Liu, K. Li, Y. Wang, H. Luo, and H. Luo, "Recent advances and trend of HEV/EV-oriented power semiconductors—An overview," *IET Power Electron.*, vol. 13, no. 3, pp. 394–404, Feb. 2020.

[28] U.-M. Choi, H.-G. Jeong, K.-B. Lee, and F. Blaabjerg, "Method for detecting an open-switch fault in a grid-connected NPC inverter system," *IEEE Trans. Power Electron.*, vol. 27, no. 6, pp. 2726–2739, Jun. 2012.

SANG-HUN KIM (Graduate Student Member, IEEE) received the B.S. degree in electrical and computer engineering from Ajou University, Suwon, South Korea, in 2019, where he is currently pursuing the M.S. degree. His research interests include grid-connected systems and electrical charger for electric vehicle.

DONG-YEON YOO (Graduate Student Member, IEEE) received the B.S. degree in electrical and computer engineering from Ajou University, Suwon, South Korea, in 2019, where he is currently pursuing the M.S. degree. His research interests include statistic-based sensor data anomaly detection and fault detection for predictive maintenance.

SANG-WON AN (Graduate Student Member, IEEE) received the B.S. degree in electrical and computer engineering from Ajou University, Suwon, South Korea, in 2019, where he is currently pursuing the M.S. degree. His research interests include multilevel inverters, grid-connected systems, and reliability.

YE-SEUL PARK (Graduate Student Member, IEEE) received the B.S. and M.S. degrees in electrical and computer engineering from Ajou University, Suwon, South Korea, in 2015 and 2017, respectively, where she is currently pursuing the Ph.D. degree with the Department of Electrical and Computer Engineering. Her research interests include fault diagnosis in predictive maintenance, statistic/ML-based sensor data analysis, ontology-based knowledge engineering, and smart factory.

JUNG-WON LEE (Member, IEEE) received the B.S. and M.S. degrees in computer science and the Ph.D. degree in computer engineering from Ewha Womans University, Seoul, South Korea, in 1993, 1995, and 2003, respectively.

She was a Research Engineer with LG Electronics, from 1995 to 1997, and completed an internship at the IBM Almaden Research Center, Data Mining Group, San Jose, CA, USA, in 2000. She was a Research Professor and a full-time Lecturer with Ewha Womans University, from 2003 to 2006. In 2006, she joined the School of Electrical and Computer Engineering, Ajou University, Suwon, South Korea. Her research interests include context-awareness, big data analysis and predictive maintenance, collaborative robots, and intelligent embedded software.

KYO-BEUM LEE (Senior Member, IEEE) received the B.S. and M.S. degrees in electrical and electronic engineering from Ajou University, Suwon, South Korea, in 1997 and 1999, respectively, and the Ph.D. degree in electrical engineering from Korea University, Seoul, South Korea, in 2003.

From 2003 to 2006, he was with the Institute of Energy Technology, Aalborg University, Aalborg, Denmark. From 2006 to 2007, he was with the Division of Electronics and Information Engineering, Jeonbuk National University, Jeonju, South Korea. In 2007, he joined the School of Electrical and Computer Engineering, Ajou University. His research interests include electric machine drives, renewable power generations, and electric vehicle applications. He is currently an Associate Editor of the IEEE TRANSACTIONS ON INDUSTRIAL ELECTRONICS, the IEEE TRANSACTIONS ON POWER ELECTRONICS, the *Journal of Power Electronics*, and the *Journal of Electrical Engineering and Technology*.